Contrast-to-Noise in X-Ray Differential Phase Contrast Imaging

Klaus J. Engel [a,*], D. Geller [a], T. Koehler [b], G. Martens [b], S. Schusser [a], G. Vogtmeier [a], E. Roessl [b]
[a] Philips Technologie GmbH – Forschungslaboratorien, Weisshausstr. 2, 52066 Aachen, Germany
[b] Philips Technologie GmbH – Forschungslaboratorien, Röntgenstr. 24-26, 22335 Hamburg, Germany
[*] Corresponding author. Tel. +49 241 6003 393, fax +49 241 6003 442. E-mail adress: klaus.j.engel@philips.com

Abstract

A quantitative theory for the contrast-to-noise ratio (CNR) in differential phase contrast imaging (DPCI) is proposed and compared to that of images derived from classical absorption contrast imaging (ACI). Most prominently, the CNR for DPCI contains the reciprocal of the spatial wavelength to be imaged, the fringe visibility, and a tunable factor dependent on the system geometry. DPCI is thus potentially beneficial especially for the imaging of small object structures. We demonstrate CNR calculations for mammography, finding optimal imaging energies between 15 and 22 keV for ACI, and between 20 and 40 keV for DPCI.

Key words: X-ray differential phase contrast imaging, grating-based interferometer, Talbot self-imaging, Contrast-to-noise ratio, mammography

1. Introduction

Hard X-ray phase contrast imaging of biological samples has proven excellent contrasts compared to common ACI [1]-[2]. According to [1], the reason is found in local variations of the refractive index

$$n = 1 - \delta - i\beta \tag{1}$$

of the imaged materials, where δ and β are the decrement of the refractive index and the absorption index, respectively. Approximately, after traversing an object, the phase modulation $\exp(i\Phi)$ and attenuation $\exp(-A)$ of an X-ray wave can be calculated in form of a path integral along a ray *s*,

$$\Phi = k_\Psi \int_s \delta(s)ds \quad \text{and} \quad A = 2k_\Psi \int_s \beta(s)ds = \int_s \mu(s)ds, \tag{2}$$

where $k_\psi = 2\pi/\lambda_\psi$ represents the wave number of the X-ray wave field Ψ with a wavelength λ_ψ, and μ represents the well-known linear X-ray attenuation coefficient (in

units of reciprocal length). In tissue the phase shift coefficient δ is typically larger than the absorption index β by about three orders of magnitude within the diagnostic X-ray energy range which explains experimentally observed strong contrasts in phase images [3]. Unfortunately, most phase contrast methods are challenging for medical imaging due to the stringent requirement of a coherent X-ray source (i.e., synchrotron radiation) and extreme mechanical stability of the setup [1]-[2]. In this context, a promising technology is seen in grating-based shearing interferometers [4], also known as Talbot interferometers [5], due to their more relaxed demands on coherency. Recent progress even allows the use of a common, polychromatic X-ray tube for a grating interferometer of the Talbot-Lau type [6]. It is an aim of this work to study the contrast-to-noise properties of this group of interferometers. As shown in more detail below, they can be distinguished from most other phase contrast methods by imaging a *differential* phase contrast related to the derivative $\partial\Phi/\partial x$ with respect to a direction *x* perpendicular to the grating lines.

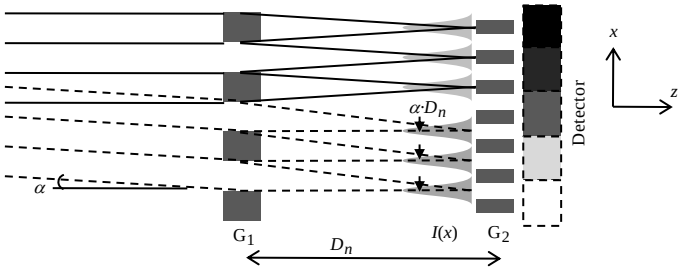

Figure 1: Schematic of a shearing interferometer.

As indicated in Figure 1, shearing interferometers are based on the self imaging of a grating G_1 according to the Talbot effect [7]. By illumination with a plane wave, an interference pattern is created at particular distances known as fractions of the Talbot distance $z_T = 2p_1^2/\lambda_\Psi$, where p_1 is the period of G_1. According to [8], self images appear periodically at distances

$$D_n = \frac{1}{\eta^2}\frac{np_1^2}{2\lambda_\Psi} \tag{3}$$

behind G_1, having a lateral fringe distance (in direction of *x*, see Figure 1) of

$$p_2 = \frac{p_1}{\eta}. \tag{4}$$

Here, *n* is the so-called Talbot order, which can be any even non-negative integer (*n* = 0, 2, 4…) for an amplitude grating and any odd positive integer (*n* = 1, 3, 5…) for a phase grating. A value of $\eta = 1$ is used for an amplitude grating or a π/2-shifting phase grating, and $\eta = 2$ is used for a π-shifting phase grating. In case that a spherical wave (instead of a plane wave) from a source with a distance *L* from G_1 is used, the interference pattern is geometrically stretched [8]. The corresponding distances d_n of the self images as well as the fringe distance p_{2n} are magnified by a factor $M_n = L/(L - D_n)$; that means that D_n and p_2 have to be substituted by $d_n = M_n \cdot D_n$ and $p_{2n} = M_n \cdot p_2$.

Usually, the fringes of the interference pattern are too small to be resolved by common X-ray detectors. For this reason, the interference pattern is scanned with an amplitude grating G_2 of similar periodicity as the fringe distance. The measured intensity of a "macroscopic" detector pixel depends on the relative positions of the local interference fringe maxima to the openings of G_2. The measured signal is thus very sensitive to lateral fringe displacements along *x* as for example caused by beam refraction within an object. Assuming that an incident wave deviates by an angle α from the grating normal in *z*-direction within the *xz*-plane (as indicated by the dashed lines in Figure 1), the fringes are displaced by $\Delta x \approx D_n \alpha$, or, as $\alpha \approx (\lambda_\psi / 2\pi) \cdot \partial\Phi/\partial x$ for a plane wave [6],

$$\Delta x \approx D_n \cdot \frac{\lambda_\psi}{2\pi} \cdot \frac{\partial \Phi}{\partial x}. \tag{5}$$

In practice, the local analysis of the fringe pattern at a detector pixel indexed by *j* is performed with a method known as "phase-shifting" [5] or "phase-stepping" [9]. For example, either G_1 or G_2 is equidistantly stepped by a number of $M_s > 2$ steps along *x* such that the fringe pattern is translated by fractions $\Delta x_g = p_2 / M_s$ of the grating period p_2. Consequently, a complete fringe period is scanned, resulting in an oscillation of the measured intensity values for each pixel. Neglecting higher harmonics [10], one can measure an intensity I_{mj} for the *m*-th phase step (with $1 \le m \le M_s$) for the *j*-th pixel

$$I_{mj} = \bar{I}_j \cdot \left[1 + \gamma_j \cdot \cos\left(\frac{2\pi \cdot m}{M_s} + \varphi_j \right) \right] \tag{6}$$

From the I_{mj}, the local mean intensity $\bar{I}_j$, the visibility γ_j, and the fringe phase φ_j can be extracted pixel-wise. For quantifying object properties, an additional reference scan has to be acquired without object, providing the quantities $\bar{I}_{j,ref}$, $\gamma_{j,ref}$ and $\varphi_{j,ref}$.

The mean intensity $\bar{I}_j$ can be used to provide an absorption image, which is calculated by

$$A_j = -\log\left(\frac{\bar{I}_j}{\bar{I}_{j,ref}} \right). \tag{7}$$

A pixel-wise differential phase contrast $\partial\Phi_j/\partial x$ (abbreviated by Φ'_j in the following) is obtained from the difference $\Delta\varphi_j = \varphi_j - \varphi_{j,ref}$ of the fringe phase offsets [9]. Using Eq. (3)-(5) one can deduce

$$\Phi'_j := \frac{\partial \Phi_j}{\partial x} \approx \frac{p_2}{D_n} \cdot \frac{\Delta\varphi_j}{\lambda} = \frac{2\eta}{n} \cdot \frac{\Delta\varphi_j}{p_1}. \tag{8}$$

This is valid for planar as well as spherical beam geometries.

In the following sections, a CNR theory is proposed which allows for predefined objects a quantitative analysis of the absorption and the differential phase contrast image. In an example, the theory is applied to mammography to derive a CNR in dependence on the photon energy for some representative cases.

2. Theory

A CNR can be derived from the contrast and the noise of a small contrast object embedded in a homogeneous larger object. The contrast object should differ from the background by $\Delta\mu$ and $\Delta\delta$ and have a topology described by a thickness function $t(x)$. We assume an illumination by a monochromatic plane wave. For ACI, the contrast object causes a difference ΔA_j in the attenuation measured by the j-th pixel (at position x_j) according to Eq. (2),

$$\Delta A_j = \Delta\mu \cdot t\left(x_j\right) = \Delta\mu \cdot t_j \,. \tag{9}$$

For DPCI, a contrast is generated dependent on the local thickness derivation $\partial t/\partial x$ with respect to x at x_j. According to Eq. (2), the contrast object causes a difference $\Delta\Phi'_j$ in the DPCI image which is

$$\Delta\Phi'_j = k_\Psi \cdot \Delta\delta \cdot \left.\frac{\partial t}{\partial x}\right|_{x=x_j} \,. \tag{10}$$

For the noise characterization, we assume that noise is solely induced for the measurements of the intensity I_{mj} for each phase step, expressed by a variance σ^2_{Imj}, i.e., we assume that the noise from any reference image should be negligible. We furthermore assume that the noise values are sufficiently small and not correlated to each other during the phase stepping such that we can use a first order noise propagation. Though very general noise sources can be used for the following analysis, we restrict ourselves to quantum (i.e., Poisson) noise to keep formulas compact. In this case, the intensity I_j is linked to a number N_j of detected photons with variance $\sigma^2_{Nj} = N_j$ via a proportionality constant c_I, resulting in

$$I_j = c_I \cdot N_j \quad \text{and} \quad \sigma^2_{Ij} = c_I^2 \sigma^2_{Nj} = c_I^2 N_j \,. \tag{11}$$

To allow a comparison between the two modalities we define a constant number $N_{ref,j}$ of available photons (i.e., incident on the object) per projection j for each image acquisition. In this case the mean number of photons detected in the j-th pixel is

$$N_j = N_{ref,j} \cdot \exp\left(-A_j\right) \cdot T_j \cdot D \,, \tag{12}$$

where T_j represents the mean transmission through any post-patient gratings (relevant for DPCI only), and D represents the detection efficiency of the detector. Applying the noise propagation for the absorption image in DPCI by using Eq. (7) and (11), one gets a variance σ^2_{Aj} for A_j which is

$$\sigma^2_{Aj} = \left(\frac{\partial A_j}{\partial \bar{I}_j}\right)^2 \sigma^2_{\bar{I}j} = \frac{\sigma^2_{\bar{I}j}}{\bar{I}_j^2} = \frac{1}{N_j} \,. \tag{13}$$

Consequently the pixel-wise CNR for an absorption image obtained from Eq. (9) and (13) is

$$CNR_{A_j} = \frac{\Delta A_j}{\sigma_{Aj}} = \Delta\mu \cdot t_j \cdot \sqrt{N_j} \,. \tag{14}$$

Applying similar noise propagation for the differential phase image with Eq. (8) and (11), one obtains

$$\sigma^2_{\Phi' j} = \left(\frac{2\eta}{np_1}\right)^2 \sigma^2_{\varphi j} = \left(\frac{2\eta}{np_1}\right)^2 \sum_{m=1}^{M_s} \left(\frac{\partial \varphi_j}{\partial I_{mj}}\right)^2 \sigma^2_{I_{mj}} = \left(\frac{2\eta}{np_1}\right)^2 \cdot \frac{2}{\gamma_j^2 N_j}, \tag{15}$$

The pixel-wise CNR for the differential phase is thus, using Eq. (10) and (15),

$$CNR_{\Phi'_j} = \frac{\Delta \Phi'_j}{\sigma_{\Phi' j}} = k_\Psi \cdot \Delta\delta \cdot \left.\frac{\partial t}{\partial x}\right|_{x=x_j} \cdot \frac{np_1}{2\eta} \cdot \gamma_j \cdot \sqrt{\frac{N_j}{2}} \,. \tag{16}$$

A quantitative comparison of the images obtained by ACI and DPCI is difficult, as both modalities show fundamentally different physical quantities. However, is it possible to "transform" the images for showing not identical, but similar contrast; for example similar object structures are expected if a "differential absorption image" (i.e., an absorption image differentiated with respect to x, $\partial A/\partial x$) is compared to the differential phase image. Vice versa, the differential phase image can be integrated along x, resulting in a phase image [6][9] which shows similar features like the absorption image. In the following we study how an absorption image compares to a phase image (= integrated differential phase image) in terms of CNR. Due to the integration, it is not sufficient to analyze single pixels but a whole detector line containing an even number N_{pix} of pixels with a pixel pitch p_d needs to be considered. We derive a phase image from the integration of the differential phase in the Fourier space. The measurements Φ'_j (with $1 \le j < N_{pix}$) of a detector line can be written in a Fourier expansion

$$\Phi'_j = c' + \sum_{k=1}^{N_{pix}/2} a'_{\Phi k} \cos\left(\omega jk + \Omega'_{\Phi k}\right) \tag{17}$$

with $\omega = 2\pi / N_{pix}$. The discrete integration with respect to x (with $x_j = jp_d$) results in

$$\Phi_j = c + jp_d c' + \sum_{k=1}^{N_{pix}/2} a_{\Phi k} \sin\left(\omega jk + \Omega'_{\Phi k}\right) \tag{18}$$

where c is an integration constant, and $a_{\Phi k} = a'_{\Phi k} \cdot p_d / \omega k$. For a comparison between ACI and integral DPCI, we study an object with a contrast insert having a periodic thickness modulation with amplitude a_{tk} and arbitrary phase offset Ω_{tk},

$$\Delta t_k(x) = a_{tk} \cdot \sin\left(\frac{2\pi \cdot x}{\lambda_k} + \Omega_{tk}\right) \tag{19}$$

with k indexing a spatial wave length $\lambda_k = N_{pix} p_d / k$ for $0 < k < N_{pix}/2$. We assume that the detector has a modulation transfer function (MTF) expressed by $T_{MTF}(\lambda_k)$. In an absorption image, the measured attenuation has a modulation amplitude a_{Ak} according to Eq. (9),

$$a_{Ak} = \Delta\mu \cdot T_{MTF}(\lambda_k) \cdot a_{tk} . \tag{20}$$

The variance σ_{Ak}^2 of a_{Ak} can be determined via error propagation of the variances $\sigma_{A_j}^2$ in an absorption image row. Assuming an object with almost constant thickness (i.e., negligible small modulation amplitude) and a homogeneous exposure, one can use a similar noise variance $\sigma_{A_j}^2 \approx \overline{\sigma_{A_j}^2} = 1/\overline{N_j}$ [see Eq. (13)] for all pixel. In this case,

$$\sigma_{Ak}^2 = \sum_{j=1}^{N_{pix}} \left(\frac{\partial a_{Ak}}{\partial A_j} \right)^2 \sigma_{A_j}^2 \approx \frac{2}{N_{pix}} \frac{1}{\overline{N_j}} = \frac{2}{N_{row}} \tag{21}$$

where N_{row} represents the total number of photons detected in a detector row. The CNR for the absorption image row is thus

$$CNR_{Ak} = \frac{a_{Ak}}{\sigma_{Ak}} = \Delta\mu \cdot T_{MTF}(\lambda_k) \cdot a_{tk} \cdot \sqrt{\frac{N_{row}}{2}} . \tag{22}$$

A similar procedure can be used for the phase image having a modulation amplitude $a_{\Phi k}$ according to the integral of Eq. (10),

$$a_{\Phi k} = k_\psi \cdot \Delta\delta \cdot T_{MTF}(\lambda_k) \cdot a_{tk} . \tag{23}$$

The variance $\sigma_{\Phi k}^2$ of $a_{\Phi k}$ is deduced from the variance $\sigma_{\Phi' k}^2$ of the corresponding modulation $a_{\Phi' k}$ in the DPCI image which in turn depends on the measured pixel variances $\sigma_{\Phi' j}^2$ in the row of the differential phase contrast image,

$$\sigma_{\Phi k}^2 = \left(\frac{p_d}{\omega k} \right)^2 \sigma_{\Phi' k}^2 = \left(\frac{p_d}{\omega k} \right)^2 \cdot \sum_{j=1}^{N_{pix}} \left(\frac{\partial a_{\Phi' k}}{\partial \phi_j} \right)^2 \sigma_{\Phi' j}^2 \approx \left(\frac{p_d}{\omega k} \cdot \frac{4\eta}{\gamma n p_1} \right)^2 \cdot \frac{2}{N_{row}} . \tag{24}$$

The CNR for the phase image row is thus

$$CNR_{\Phi k} = \frac{a_{\Phi k}}{\sigma_{\Phi k}} = k_\psi \cdot \Delta\delta \cdot T_{MTF}(\lambda_k) \cdot a_{tk} \cdot \frac{2\pi}{\lambda_k} \cdot \gamma \cdot \frac{n p_1}{4\eta} \cdot \sqrt{\frac{N_{row}}{2}} . \tag{25}$$

Comparing the CNR for the absorption and for the phase image row, Eq. (22) and (25), one notices that both contain an identical term $T_{MTF}(\lambda_k) \cdot a_{tk} \cdot \sqrt{\frac{N_{row}}{2}}$, which represents the object topology and the quantum noise. The material contrasts are represented by the terms $\Delta\mu$ and $k_\psi \cdot \Delta\delta$ in the absorption and the phase image, respectively. The CNR for the phase image, however, contains essentially three additional terms which are not

present in the CNR of the absorption image, that is firstly the reciprocal $2\pi/\lambda_k$ of an imaged spatial wavelength of the contrast object, secondly, the visibility γ, and thirdly, a geometrical factor $np_1/4\eta$. From $2\pi/\lambda_k$ one concludes that DPCI is the more advantageous over ACI, the smaller the wavelength of a contrast structure is (limited however by the detector MTF and the pixel width p_d). The visibility factor γ makes clear that a loss of coherency (caused by the system or by the object) linearly degrades the CNR of the phase image, but not that of the absorption image. Finally, the CNR of the phase image can be tuned by varying the Talbot order n or the grating pitch p_1.

3. Methods and Results

We demonstrate how theoretical CNR results can be applied for mammography, where we assume that contrast is generated by mutual substitution of water and lipid [11]. We used two breast phantoms, represented by slices of 2 cm and 8 cm thickness, covering upper and lower extreme cases in mammography. The energy-dependent X-ray coefficients μ and δ are calculated according to [12] using data tables of [13]. In a first example, the dependency of the CNR on the photon energy E is analyzed. The purpose is to find an optimal (monochromatic) E, for which the CNR is maximized under the boundary condition of a constant total energy deposition E_{dose} in the breast. The constant dose assumption implies that the number $N_{ref}(E)$ of photons incident on the phantom is a function of E; for a mean energy deposition of $E_{dep}(E)$ per photon one gets $N_{ref}(E) = E_{dose}/E_{dep}(E)$. The function E_{dep} is determined statistically by Monte Carlo X-ray scattering simulations with a tool described in [14]. Eq. (22) can be rewritten in the form

$$CNR_{Ak} = CNR_A(E)\cdot T_{MTF}(\lambda_k)\cdot a_{tk}\cdot\sqrt{E_{dose}} \text{ with} \tag{26}$$

$$CNR_A(E) = \Delta\mu(E)\sqrt{\frac{D(E)\cdot T(E)\cdot\exp(-\mu_b(E)t_b)}{2E_{dep}(E)}} \tag{27}$$

with the substitution $N_{row}(E) = N_{ref}(E)\cdot D(E)\cdot T(E)\cdot\exp(-\mu_b(E)t_b)$, wherein D is the detector quantum efficiency, T is the grating transmission, and $\mu_b(E)\cdot t_b$ is the breast phantom attenuation. Accordingly, Eq. (25) is rewritten to

$$CNR_{\Phi k} = CNR_\Phi(E)\cdot T_{MTF}(\lambda_k)\cdot a_{tk}\cdot\frac{2\pi}{\lambda_k}\cdot\frac{np_1}{4\eta}\cdot\sqrt{E_{dose}} \text{ with} \tag{28}$$

$$CNR_\Phi(E) = \frac{2\pi E}{hc}\cdot\Delta\delta(E)\cdot\gamma(E)\cdot\sqrt{\frac{D(E)\cdot T(E)\cdot\exp(-\mu_b(E)t_b)}{2E_{dep}(E)}} \tag{29}$$

using $k_\Psi = 2\pi E/hc$ with $hc = 1.24\cdot10^{-9}\,keV\cdot m$. In Figure 2 and Figure 3, $CNR_A(E)$ and $CNR_\Phi(E)$ are plotted for thicknesses t_b = 2 cm and t_b = 8 cm, respectively, where for

$\Delta\mu(E)$ and $\Delta\delta(E)$ the corresponding difference functions between the materials water and lipid and for $\mu_b(E)$ the material "breast – mammary gland type 2" were used [11]. We assumed a constant visibility $\gamma = 1$ for all energies. For the ideal system case, $D = T = 1$ were used; for the more realistic detector scenarios, a function $D(E)$ was simulated with the Monte Carlo tool for a Se detector of 200 µm thickness and several CsI detectors with thicknesses of 150, 300, and 600 µm. For $CNR_A(E)$, a constant transmission of $T = 1$ was assumed; for $CNR_\Phi(E)$, the transmission $T(E)$ through a 100 µm thick grating G_2 with absorbing trenches consisting of Au and openings consisting of Si was calculated.

A quantitative comparison between the CNR of ACI and integral DPCI, normalized by $a_{tk} \cdot \sqrt{E_{dose}}$, is shown in Figure 4 for a specified setup using n=1, η=2, and p_1=5.7 µm, with the same 8 cm thick breast phantom as used in Figure 3.We assumed an ideal MTF with $T_{MTF} = 1$, a grating transmission of $T = 0.5$ (i.e. ideal absorbers), and an ideal visibility of $\gamma = 1$.

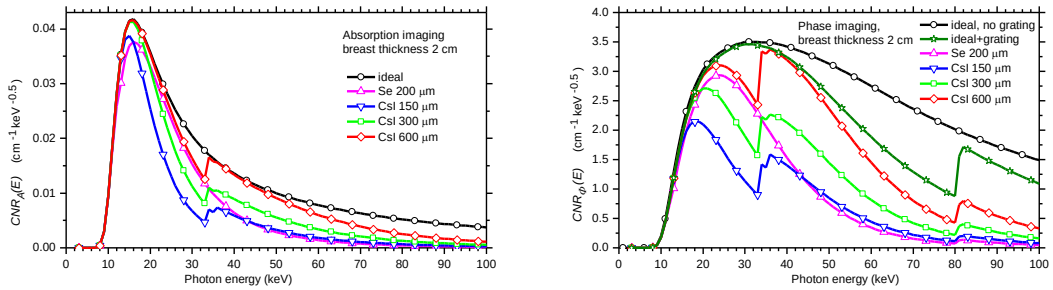

Figure 2: CNR dependency on photon energy for a 2 cm thick breast phantom under assumption of a constant-dose scenario with monochromatic radiation. Left: CNR for ACI; right: corresponding CNR for DPCI with system geometries optimized for each *E*. Black: ideal system, colors: use of detectors with limited quantum efficiency (Se or CsI with various thicknesses), in case of DPCI also with realistic gratings.

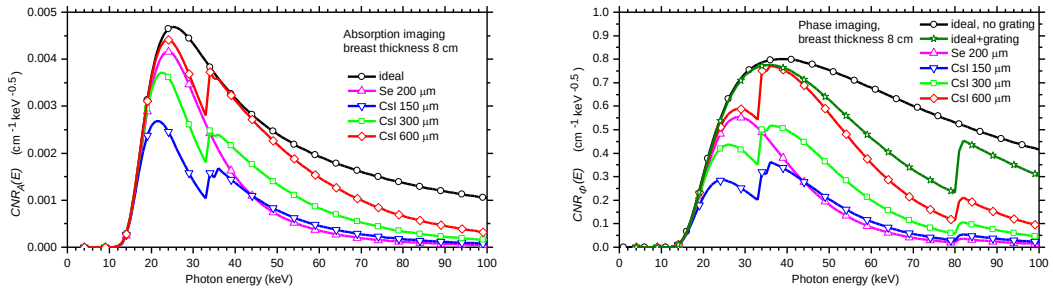

Figure 3: As Figure 2, but for an 8 cm thick breast phantom.

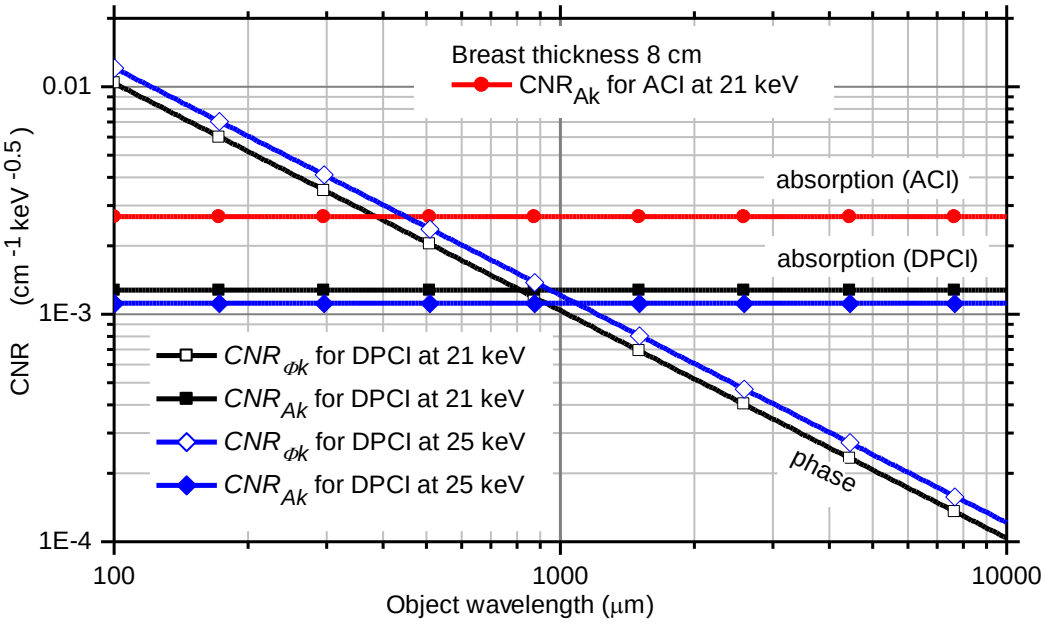

Figure 4: Quantitative CNR for DPCI and ACI for the 8 cm thick breast phantom, plotted versus an spatial wavelength λ_k of a contrast object structure (lipid in water), for photon energies of 21 keV and 25 keV.

4. Discussion

Looking at Figure 2 and Figure 3, it is evident that there exists an optimal energy range between 15 and 22 keV for ACI (agreeing to commonly used X-ray spectra for mammography) and between 20 and 40 keV for integral DPCI. For CsI detectors, a CNR "gap" is seen below 34 keV which is due to a weaker X-ray absorption below the K-edges of Cs and I, and thus a weaker quantum efficiency. A very low CNR is found for energies below 15 or 20 keV for the 2 cm and 8 cm breast phantoms, respectively, as the strong object absorption causes photon starvation. For very high energies, in both modalities the CNR again decreases, for ACI more rapidly than for integral DPCI. The main limiting factor in ACI is identified in the energy dependence of $\Delta\mu$, which rapidly decreases with E. In integral DPCI, $k_\psi \Delta\delta$ also decreases with $1/E$ [12], but not as rapidly as $\Delta\mu$ which explains why the optimal energy range for integral DPCI is shifted towards higher energies. In both modalities, the CNR is further degraded for increased energies as the detector efficiency decreases above 50 keV. For integral DPCI it has to be noted that $\gamma = 1$ was assumed in the calculations for Figure 2 and Figure 3, but in practice an absorber grating becomes more transparent for higher energies and thus degrade the visibility. For a fair comparison, one must thus multiply the $CNR_\Phi(E)$ curves with a realistic $\gamma(E)$ dependency. In summary, for a potential DPCI setup, it seems reasonable

to choose design energies around 25 keV, as at this energy a best compromise is found for the CNR of all images.

Analyzing Figure 4, it is evident that DPCI could potentially serve as an improved imaging of the fine structure of an object. ACI clearly differs from DPCI as there is no direct dependency of CNR_{Ak} on a spatial wavelength. In contrast, $CNR_{\Phi k}$ shows the $1/\lambda_k$ dependency as indicated in Eq. (25). Consequently there is found a characteristic spatial wavelength λ_c below which DPCI shows a CNR superior to that of ACI. In the shown example this is the case for $\lambda_c < 400$ µm. However, λ_c is influenced by a lot of variables. Negative influencing variables for DPCI (shifting the CNR curve downwards in Figure 4) are in the first place the visibility, which is not only affected by the experimental setup (with typical values $\gamma < 0.4$), but can also be further reduced by the scattering properties of the object itself [15]. Two very essential variables are furthermore given by $k_\psi \Delta\delta$ and $\Delta\mu$. Choosing other contrast material combinations can significantly scale the CNR curves of both modalities in Figure 4.

5. Summary

A quantitative contrast-to-noise (CNR) theory for absorption contrast imaging (ACI) and differential phase contrast imaging (DPCI) was presented. The CNR for the phase image (as an integral DPCI image) contains essentially three additional factors which are not present in the CNR of the absorption image, that is the reciprocal $2\pi/\lambda_k$ of an imaged wavelength of the contrast object, the visibility γ, and a geometrical factor proportional to the Talbot order and the periodicity of grating G_1. Phase contrast imaging is thus potentially beneficial especially for the imaging of small object structures. The theoretical results were applied to find an optimal photon energy for ACI in the range between 15 and 22 keV, and for DPCI in the range between 20 and 40 keV. In an example calculation for a 8 cm thick breast phantom, it is found that lipid/water contrasts can potentially be imaged by DPCI with an improved CNR for object structures below 400 µm.

Acknowledgements

We gratefully acknowledge helpful discussions with Nicholas Blanc, Christian Kottler, and Rolf Kaufmann from the Centre Suisse d'Electronique et de Microtechnique (CSEM).

References

[1] R.A. Lewis, Phys. Med. Biol. 49 (2004) 3573-3583.

[2] A. Momose, Jpn. J. Appl. Phys. 44 (2005) 6355-6367.

[3] T.J. Davis, D. Gao, T.E. Gureyev, A.W. Stevenson, S.W. Wilkins, Nature 373 (1995) 595-598.

[4] C. David, B. Nöhammer, H.H. Solak, Appl. Phys. Lett. 81 (2002) 3287-3289.

[5] A. Momose, S. Kawamoto, I. Koyama, Y. Hamaishi, K. Takai, Y. Suzuki, Jpn. J. Appl. Phys. 42 (2003) L866-L868.

[6] F. Pfeiffer, T. Weitkamp, O. Bunk, C. David, Nat. Phys. 2 (2006) 258-261.

[7] P. Cloetens, J.P. Guigay, C. De Martino, J. Baruchel, M. Schlenker, Opt. Lett. 22 (1997) 1059-1061.

[8] T. Weitkamp, C. David, C. Kottler, O. Bunk, F. Pfeiffer, Proc. SPIE 6318 (2006) 63180S, 1-9.

[9] T. Weitkamp, A. Diaz, B. Nöhammer, F. Pfeiffer, T. Rohbeck, P. Cloetens, M. Stampanoni, C. David, Proc. SPIE 5535 (2004) 137-142.

[10] A. Momose, S. Kawamoto, I. Koyama, Y. Suzuki, Proc. SPIE 5535 (2004) 352-360.

[11] ICRU Report 46 of the International Commission on Radiation Units and Measurements, Bethesda, MD (1989)

[12] B.L. Henke, E.M. Gullikson, J.C. Davis, At. Data Nucl. Data Tables 54 (1993) 181-342.

[13] C.T. Chantler, J. Phys. Chem. Ref. Data 29 (2000) 597-1048.

[14] S.M. Schneider, J.P. Schlomka, G. Harding, Proc. SPIE 4320 (2001) 754-763.

[15] F. Pfeiffer, M. Bech, O. Bunk, P. Kraft, E.F. Eikenberry, Ch. Brönnimann, C. Grünzweig, C. David, Nat. Mater. 7 (2008) 134-137.